

RectifiedHR: Enable Efficient High-Resolution Image Generation via Energy Rectification

Zhen Yang^{1*} Guibao Shen^{1*} Liang Hou² Mushui Liu⁴ Luozhou Wang¹
 Xin Tao² Pengfei Wan² Di Zhang² Ying-Cong Chen^{1,3†}
¹HKUST(GZ) ²Kuaishou Technology ³HKUST ⁴Zhejiang University
 {zheny.cs, sgbsiat, wileewang97, jiangsutx}@gmail.com, lms@zju.edu.cn
 {houliang06, wanpengfei, zhangdi08}@kuaishou.com, yingcongchen@ust.hk



Figure 1. Generated images of our method. Our training-free method can enable diffusion models (SDXL in the figure) to generate images at resolutions higher than their original training resolution. **ZOOM IN** for a closer look.

Abstract

Diffusion models have achieved remarkable advances in various image generation tasks. However, their performance notably declines when generating images at resolutions higher than those used during the training period. Despite the existence of numerous methods for producing high-resolution images, they either suffer from inefficiency or are hindered by complex operations. In this paper, we propose RectifiedHR, an efficient and straightforward solution for training-free high-resolution image generation. Specifically, we introduce the noise refresh strategy, which theoretically only requires a few lines of code to unlock the model’s high-resolution generation ability and improve efficiency. Additionally, we first observe the phenomenon of energy decay that may cause image blurriness during the high-resolution image generation process. To address this issue, we propose an Energy Rectification strategy, where

modifying the hyperparameters of the classifier-free guidance effectively improves the generation performance. Our method is entirely training-free and boasts a simple implementation logic. Through extensive comparisons with numerous baseline methods, our RectifiedHR demonstrates superior effectiveness and efficiency. The project page can be found [here](#).

1. Introduction

The development of diffusion models [6, 11, 26, 29, 33, 36, 40, 42, 58] has made the generative artificial intelligence community more prosperous, which has also improved the performance of a large number of visual tasks, such as image editing [1, 4, 8, 24, 38, 39, 52, 54] and custom generation [2, 9, 12, 28, 44, 51]. Although the models perform well on these tasks, due to the lack of train-

*Equal contribution. †Corresponding author.

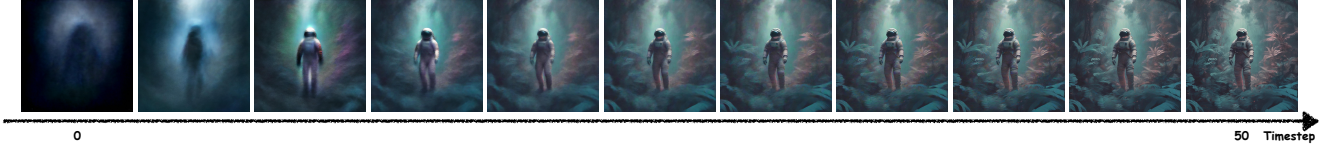


Figure 2. The visualization results of predicted x_0 at different time step t , abbreviated as $p_{x_0}^t$. The figure visualizes the process of how $p_{x_0}^t$ changes with the sampling steps, where the x-axis represents the timestep in the sampling process. The 11 images are evenly extracted from 50 images. It can be observed that in the first half of the process, $p_{x_0}^t$ is mainly responsible for global structure generation, while the second half is mainly responsible for local detail generation.

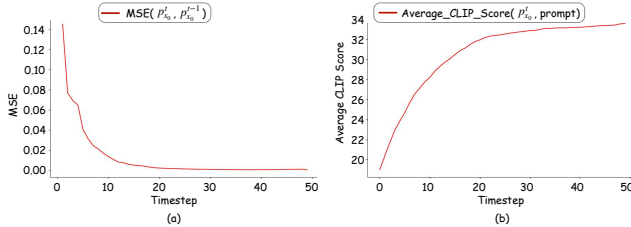


Figure 3. The trend of predicted x_0 at different time step t , abbreviated as $p_{x_0}^t$, on 100 random prompts. (a) The trend of the average CLIP Score between $p_{x_0}^t$ and the prompt over different timesteps. The x-axis represents the sampling timestep, and the y-axis represents the average CLIP Score. (b) Average MSE between $p_{x_0}^t$ and $p_{x_0}^{t-1}$. The x-axis represents the sampling timestep, and the y-axis represents the Average MSE. It can be observed that after approximately 30 steps, the trend of change in $p_{x_0}^t$ slows down.

ing in high-resolution data, existing methods show a performance drop when generating images beyond the resolution of the training data. Training on high-resolution images is costly, so unleashing the model’s capability to generate high-resolution images without additional training has become important.

Currently, many methods have explored training-free high-resolution generation task. These methods have attempted a variety of complex techniques, including schemes based on sliding window denoising [2, 10, 27, 30, 31], modifying the model network structure [14, 20, 22, 56], adjusting classifier-free guidance [13, 21]. Some methods design suitable prompts for high-resolution image generation using vision language models [35, 47]. Others leverage the idea of image editing capabilities [37] to enrich the details of low-resolution images [5, 25, 53, 57]. However, these methods either require redundant sampling steps, leading to efficiency issues, suffer from repetitive patterns due to insufficient global information exchange, or have complex implementation logic. This raises an important question: Can we create a method that is efficient and has simple implementation logic?

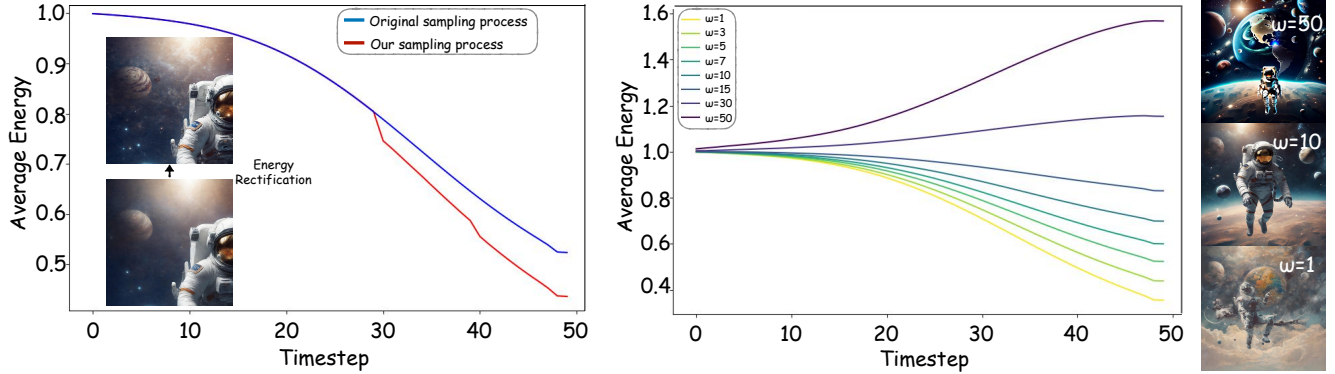
In this work, we propose RectifiedHR, a simple and efficient framework for high-resolution image generation. Our approach consists of two modules: noise refresh and en-

ergy rectification. Specifically, Noise Refresh enhances the resolution of “predicted x_0 ” at certain sampling steps in the diffusion model and introduces new noise to align with the current step. Gradually applying noise refresh enables coarse-to-fine high-resolution image generation. Noise Refresh preserves the original sampling steps to ensure efficient performance. Consequently, our method achieves a significant speed advantage compared to approaches like DiffuseHigh[25] and AP-LDM[5], which rely on multi-round editing, as well as Signal-to-Noise Ratio (SNR) correction schemes such as FreCas[57] and MegaFusion[53], all of which introduce extra sampling steps. Furthermore, we observe an energy decay phenomenon in Noise Refresh and mitigate this issue by increasing the classifier-free guidance (CFG)[17] hyperparameter for energy rectification. As demonstrated in Fig. 5, our approach achieves superior results through a simple and efficient framework.

Concretely, we observe in Fig. 2 and Fig. 3 that “predicted x_0 ” primarily generates structure in early sampling steps and details in later sampling steps. Since low-resolution image details are lost during resizing, they contribute little to high-resolution images. Thus, in later sampling stages, we progressively replace low-resolution images with high-resolution ones. This preserves structural information from low resolutions to reduce repetitive patterns while skipping unnecessary low-resolution detail generation, enabling an efficient noise refresh algorithm. However, as shown in Fig. 7, using Noise Refresh alone introduces blurriness. To analyze the source of the issue, we introduce latent average energy to measure energy changes during sampling. As illustrated in Fig. 4a, we observe that Noise Refresh induces energy decay. We further discover that CFG (Classifier-Free Guidance) can control the latent average energy, as demonstrated in Fig.4b. Therefore, we can achieve energy rectification simply by increasing the value of the CFG hyperparameter, ensuring that RectifiedHR achieves high speed, superior quality, and straightforward logic.

In general, our main contributions are as follows:

- We introduce relative latent energy analysis, and to the best of our knowledge, we are the first to discover the energy decay phenomenon during the high-resolution gen-



(a) The energy decay phenomenon of our noise refresh sampling process compared to the original sampling process on 100 random prompts.

(b) The process of how the average latent energy changes with the timestep when 1024 x 1024 resolution images are generated from 100 random prompts under different classifier-free guidance hyperparameters.

Figure 4. (a) The x-axis represents the timestep of the sampling process, and the y-axis represents the average latent energy. The blue line shows the average latent energy of the original sampling process generating 1024 x 1024-resolution images over the sampling process. The red line represents our noise refresh sampling process, where noise refresh is performed at the 30th and 40th sampling timesteps, and the resolution gradually increases from 1024 x 1024 to 2048 x 2048, and then to 3072 x 3072. It can be observed that noise refresh will cause the relative latent energy to show a significant decay. From the left images, it can be observed that after energy rectification, the image details have become more prominent. (b) The x-axis represents the timestep, the y-axis represents the average latent energy, and ω is the hyperparameter for classifier-free guidance. It can be observed that the relative latent energy increases with the increase of ω . From the right figures, it can be observed how the images change as ω increases.

eration process.

- We design a novel training-free high-resolution image generation pipeline, which primarily includes noise refresh and energy rectification operations. This pipeline requires fewer lines of theoretical code to implement and is highly efficient.
- We compare RectifiedHR with a large number of existing baselines and demonstrate the efficiency and effectiveness of our approach.

2. Related Work

2.1. Text-guided image generation

With the scaling of models, data volume and computational resources, text-guided image generation models have witnessed unprecedented growth, leading to the emergence of numerous diffusion models, including LDM [42], SDXL [40], PixArt [6, 7], HunyuanDiT [29], LuminaNext [58], FLUX [26], SD3 [11] and LCM [36]. These models establish connections between Gaussian noise and high-quality images through various training and sampling methods, such as DDPM [18], SGM [50], EDM [23], DDIM [49], flow matching [32] and rectified flow [34]. However, due to the lack of training on high-resolution data, these models exhibit optimal performance only at specific resolutions and fall short when generating images with higher resolution. Consequently, exploring the potential of diffusion models for high-resolution image generation in a training-free manner has become crucial in the vision-generation community.

Our approach focuses primarily on achieving efficient high-resolution image generation with minimal modifications to existing pipelines.

2.2. Training-free high-resolution image generation

Due to the domain gap between different resolutions, directly using diffusion models for high-resolution image generation can result in pattern repetition and poor semantic structure. MultiDiffusion [2] proposes a sliding window denoising scheme to achieve panoramic image generation. However, this method suffers from serious pattern repetition issues, as it mainly considers the aggregation of local information. Improved methods based on the sliding window denoising scheme include SyncDiffusion [27], Demofusion [10], AccDiffusion [31], and CutDiffusion [30]. Specifically, SyncDiffusion introduces global information using the gradient of perceptual loss from the predicted denoised images at each denoising step as guidance. Demofusion uses progressive upscaling, skip residual, and dilated sampling mechanisms to achieve higher-resolution image generation. AccDiffusion’s patch-content-aware prompts mechanism and CutDiffusion’s coarse-to-fine mechanism can solve pattern repetition issues. But they all have complex implementation logic and suffer from efficiency issues. ScaleCrafter [14], FouriScale [20], HiDiffusion [56], and Attn-SF[22] modify the network structure of the diffusion model, which may lead to suboptimal performance. Additionally, ScaleCrafter, FouriScale, and HiDiffusion can not generalize to other UNet[43]-free diffusion models be-

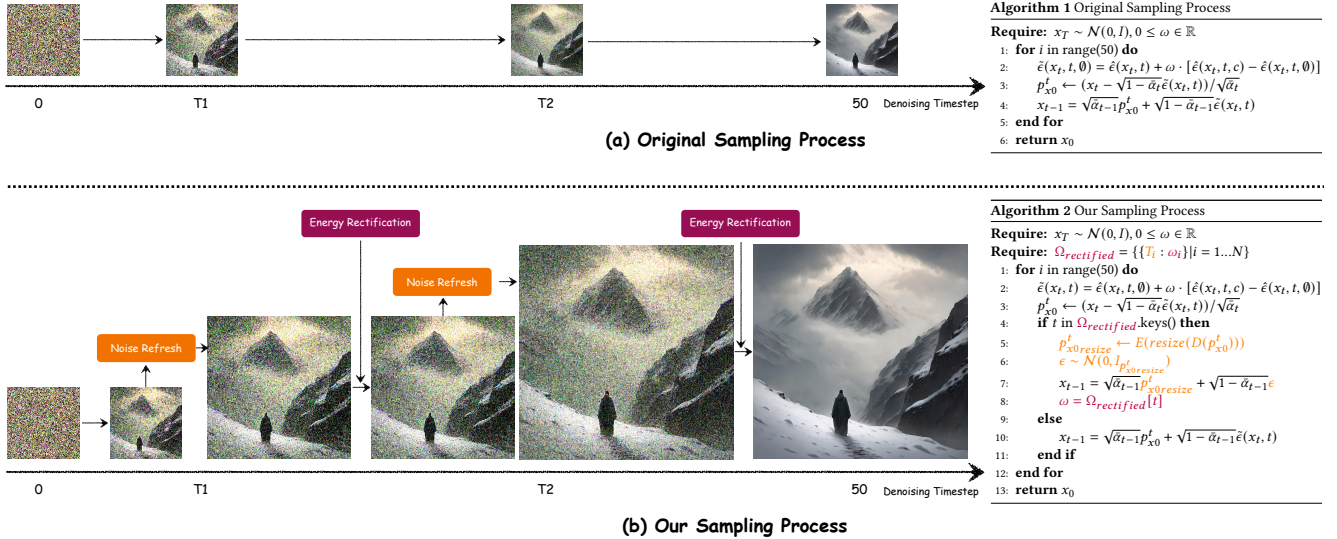


Figure 5. Overview of our method. (a) the original sampling process and its pseudocode. (b) The sampling process and pseudocode of our method. The orange parts of the pseudocode and modules correspond to **Noise Refresh**, while the purple parts represent **Energy Rectification**. ϵ is a Gaussian random noise and its shape changes according to the shape of $p_{x_0}^{i,resize}$. Other symbols in the pseudocode can be found in Sec.3.1.

cause of their highly structure-related methods. ResMaster [47] and HiPrompt [35] introduce multi-modal models to regenerate prompts to enrich image details, but the introduction of multi-modal models is too heavy, resulting in further efficient problems. Upscale Guidance [21] and ElasticDiffusion [13] all propose to add global denoising information and local denoising information to classifier-free guidance [17]. However, their global information requires heavy computational complexity compared to our progressive resolution increase approach. DiffuseHigh [25] and AP-LDM [5] utilize SDEdit’s [37] detail enhancement capability, gradually adding details from low-resolution images to high-resolution images. Compared to these methods, our approach does not increase the sampling steps and is therefore more efficient, while also having a simple implementation. The most related concurrent works to ours are FreCas [57] and MegaFusion [53]. Compared to rescale noise methods like FreCas and MegaFusion, our method only modifies fewer lines of the sampling formula, resulting in a simpler implementation logic while also avoiding the need for additional sampling steps. Compared to FreCas, we discover the energy decay issue and only need to adjust the classifier-free guidance parameter to rectify the energy to achieve better results.

3. Method

3.1. Preliminaries

The diffusion models establish a connection between Gaussian noise and images, enabling the generation of an image

by randomly sampling a noise. In this paper, we default to using SDXL [40] for our experiments and we assume the sampling steps to be 50 steps, with the denoising process defaulting from step 0 to step 49. We define I_o as the real RGB image. During the training process, SDXL first adopts a VAE encoder $E(\cdot)$ to transform the RGB image into a lower-dimensional latent space, and we refer to the transformed latent as x_0 . Then, by applying the forward diffusion formula as follows:

$$x_t = \sqrt{\bar{\alpha}_t} x_0 + \sqrt{1 - \bar{\alpha}_t} \epsilon, \quad (1)$$

we add varying degrees of noise to x_0 to obtain different x_t , where $\bar{\alpha}_t$ is a time-related scheduler parameter to control the noise strength and ϵ is a random sampled Gaussian noise. The neural network $\hat{\epsilon}(x_t, t, c)$ parameterized by θ is optimized to predict the noise added to x_0 by the following training objective:

$$\min_{\theta} \mathbb{E}_{x_t, t, c} \left[\|\epsilon - \hat{\epsilon}(x_t, t, c)\|_2^2 \right], \quad (2)$$

where c is the condition signal for generation (text prompt for T2I task). During the sampling process, random noise is sampled in the latent space, and then the diffusion model transforms the random noise into an image in a gradually denoise manner. Finally, the latent is passed through a VAE’s decoder $D(\cdot)$ to reconstruct a generated RGB image. The objective of high-resolution generation is to generate images with resolutions beyond the training dataset’s, e.g. resolutions more than 1024 x 1024 in our setting.

Classifier-free guidance for diffusion models. Currently, classifier-free guidance (CFG) [17] is widely used to enhance the quality of generated images by incorporating unconditional output at each denoising step. The classifier-free guidance formula is as follows:

$$\tilde{\epsilon}(x_t, t) = \hat{\epsilon}(x_t, t, \emptyset) + \omega \cdot [\hat{\epsilon}(x_t, t, c) - \hat{\epsilon}(x_t, t, \emptyset)], \quad (3)$$

where ω is the hyperparameter of classifier-free guidance, $\hat{\epsilon}(x_t, t, \emptyset)$ and $\hat{\epsilon}(x_t, t, c)$ represent the predicted noises of the unconditional branch and conditional branch respectively, we refer to $\tilde{\epsilon}(x_t, t)$ as the predicted noise after applying classifier-free guidance.

Sampling process for diffusion models. In this paper, we use the DDIM sampler [49] by default. The deterministic sampling formula for DDIM is as follows:

$$x_{t-1} = \sqrt{\bar{\alpha}_{t-1}} \left(\underbrace{\frac{x_t - \sqrt{1 - \bar{\alpha}_t} \tilde{\epsilon}(x_t, t)}{\sqrt{\bar{\alpha}_t}}}_{\text{predicted } x_0 \rightarrow p_{x_0}^t} \right) + \sqrt{1 - \bar{\alpha}_{t-1}} \cdot \tilde{\epsilon}(x_t, t), \quad (4)$$

As illustrated in Eq. 4, in time step t , we first predict the noise $\tilde{\epsilon}(x_t, t)$ by the pre-trained neural network $\hat{\epsilon}(\cdot)$. Then, we can compute a predicted “ x_0 ” at time step t called $p_{x_0}^t$. Finally, x_{t-1} could be derived from $\tilde{\epsilon}(x_t, t)$ and $p_{x_0}^t$ by the diffusion process in Eq. 4.

3.2. Noise refresh

As shown in the changes of $p_{x_0}^t$ with timestep t in Fig. 2, we can observe that during the first half of the denoising process, the global structural information of $p_{x_0}^t$ undergoes significant changes. However, in the latter half, the global structure remains largely unchanged, with the primary focus shifting toward the generation of detailed local information. As shown in Fig. 3, we further conduct experiments on the generation of $p_{x_0}^t$ on 100 random prompts from LAION-5B [46] and analyze the CLIP Score [15] and Mean Squared Errors (MSE). In Fig. 3b, it is observed that after 30 steps of denoising, the CLIP score of $p_{x_0}^t$ with prompt increases slowly. From Fig. 3a, we find that after 30 steps of denoising, the MSE between $p_{x_0}^t$ and $p_{x_0}^{t-1}$ changes very little. Therefore, we consider that the latter stages of the denoising process are primarily responsible for generating finer details. Furthermore, we find that in the last half of the sampling process, the global structure of $p_{x_0}^t$ remains largely unchanged. Therefore, we can convert $p_{x_0}^t$ to the RGB space for resizing. In addition, the latter sampling stage is mainly responsible for the generation of local details. Based on the above two points, we can generate high-resolution images with rich details. The formula for increasing the resolution of the $p_{x_0}^t$ is as follows:

$$p_{x_0 \text{ resize}}^t = E(\text{resize}(D(p_{x_0}^t))), \quad (5)$$

where E represents VAE’s Encoder, and *resize* refers to the operation of increasing the size of the RGB image. We adopt the bilinear interpolation as the default resize operation. Directly changing the size of x_t can cause Signal-to-Noise Ratio (SNR) mismatch issues [19, 21]. Therefore, we have updated the sampling formula to refresh a new noise. The updated sampling formula is as follows:

$$x_{t-1} = \sqrt{\bar{\alpha}_{t-1}} p_{x_0 \text{ resize}}^t + \sqrt{1 - \bar{\alpha}_{t-1}} \epsilon \quad (6)$$

ϵ represents a random Gaussian noise that shares the same shape as $p_{x_0 \text{ resize}}^t$. We refer to this process as **Noise Refresh**.

As illustrated in Fig. 5b, the noise refresh operation is applied to several specific time points T_i during the sampling process. To automate the selection of these time steps T , we propose the following selection formula:

$$T_i = (T_{max} - T_{min}) * \left(\frac{i}{N}\right)^M + T_{min}, \quad (7)$$

T_{max} and T_{min} define the range of sampling timesteps to use noise refresh. N denotes the number of noise refresh that need to be performed. The range of i is all integers between 1 and N . M is a hyperparameter that can be adjusted to obtain different strategies to select T_i .

3.3. Energy rectification

Although the image resolution increases after using noise refresh, we find that the generated images exhibit significant blurring if we do not conduct further process, as shown in the fourth column in Fig. 7. To analyze the cause of this phenomenon, we introduce relative latent energy formula as follows:

$$Ex_t^2 = \frac{\sum_{i=1}^C \sum_{j=1}^H \sum_{k=1}^W x_{t_{ijk}}^2}{C \times H \times W}, \quad (8)$$

x_t represents the latent variable at time t , where C , H , and W denote the dimensions of the channel, height, and width of latent, respectively. The definition is very similar to the energy definition of an image, and is used to indicate the average energy of each element of a latent vector.

To analyze the issue of image blurring, we conduct an average energy experiment on 100 random prompts. As illustrated in Fig. 4a, we first compare the relative latent energy differences between the noise refresh sampling process and the original sampling process. We observe a significant energy decay phenomenon in the noise refresh sampling process, which is the reason why the naive implementation method produces noticeably blurred images. Subsequently, we conduct an experiment to analyze the impact of the hyperparameter ω in classifier-free guidance on latent energy. As shown in Fig. 4b, we find that as the classifier-free guidance parameter ω increases, the energy exhibits a



Figure 6. Qualitative comparison of our method with other training-free methods using three LAION-5B’s prompts.

gradually increasing trend. Therefore, we can address the issue of energy decay and improve the quality of generated images by increasing ω to enhance the energy in the noise refresh sampling scheme. As demonstrated in the fourth column and fifth column in Fig. 7, after the energy is rectified with a larger classifier-free guidance hyperparameter ω , the blurry issue has been well addressed and the generated image shows remarkable clarity. We refer to this process of correcting energy decay as **Energy Rectification**.

As shown in Fig. 5b, the energy rectification operation is applied to the sampling process after noise refresh. To more automatically select ω in the classifier-free guidance, we propose the following selection formula:

$$\omega_i = (\omega_{max} - \omega_{min}) * \left(\frac{i}{N}\right)^M + \omega_{min}, \quad (9)$$

ω_{max} and ω_{min} represent the range of ω in classifier-free

guidance during sampling process. N denotes the number of noise refresh that needs to be performed. The range of i is all integers between 1 and N . M is a hyperparameter that can be adjusted to obtain different strategies to select ω_i .

4. Results

4.1. Evaluation Setup

We conduct experiments using SDXL [40] with 50 sampling steps as our base model, which is able to generate images at 1024 x 1024 resolution by default. Following the previous work, we randomly sample 1,000 prompts from the laion-5B [46] dataset as conditions to generate images. We compare our method with the following state-of-the-art: Demofusion [10], DiffuseHigh [25], HiDiffusion[56], Cut-Diffusion [30], ElasticDiffusion [13], AP-LDM [5], FreCas [57], SDXL+BSRGAN [55] FouriScale [20], ScaleCrafter

	Methods	FID _r ↓	KID _r ↓	IS _r ↑	FID _c ↓	KID _c ↓	IS _c ↑	CLIP↑	Time↓
2048x2048	FouriScale	71.344	0.010	15.957	53.990	0.014	20.625	31.157	59s
	ScaleCrafter	64.236	0.007	15.952	45.861	0.010	22.252	31.803	35s
	HiDiffusion	63.674	0.007	16.876	41.930	0.008	23.165	31.711	18s
	CutDiffusion	59.152	0.007	17.109	38.004	0.008	23.444	32.573	53s
	ElasticDiffusion	56.639	0.010	15.326	37.649	0.014	19.867	32.301	150s
	AP-LDM	51.083	0.004	18.867	29.193	0.006	25.331	33.601	25s
	AccDiffusion	48.143	0.002	18.466	32.747	0.008	24.778	33.153	111s
	DiffuseHigh	49.748	<u>0.003</u>	19.537	27.667	<u>0.004</u>	27.876	33.436	37s
	FreCas	49.129	<u>0.003</u>	20.274	27.002	<u>0.004</u>	29.843	33.700	14s
	DemoFusion	47.079	0.002	19.533	26.441	<u>0.004</u>	27.843	33.748	79s
	SDXL+BSRGAN	<u>47.452</u>	0.002	<u>20.260</u>	<u>25.827</u>	<u>0.004</u>	27.155	33.867	6s
Ours	48.361	0.002	20.616	25.347	0.003	<u>28.126</u>	33.756	13s	
4096x4096	FouriScale	135.111	0.046	9.481	129.895	0.057	9.792	26.891	489s
	ScaleCrafter	110.094	0.028	10.098	112.105	0.043	11.421	27.809	528s
	HiDiffusion	93.515	0.024	11.878	120.170	0.058	11.272	27.853	71s
	CutDiffusion	130.207	0.055	9.334	113.033	0.055	10.961	26.734	193s
	ElasticDiffusion	101.313	0.056	9.406	111.102	0.089	7.627	27.725	400s
	AP-LDM	51.274	0.005	18.676	41.615	0.012	20.126	<u>33.632</u>	153s
	AccDiffusion	54.918	0.005	17.444	60.362	0.023	16.370	32.438	826s
	DiffuseHigh	48.861	<u>0.003</u>	19.716	40.267	<u>0.010</u>	<u>21.550</u>	33.390	190s
	FreCas	49.764	<u>0.003</u>	18.656	39.047	<u>0.010</u>	21.700	33.237	74s
	DemoFusion	48.983	<u>0.003</u>	18.225	<u>38.136</u>	<u>0.010</u>	20.786	33.311	605s
	SDXL+BSRGAN	47.923	0.002	<u>19.815</u>	41.126	0.014	19.231	33.874	6s
Ours	48.684	<u>0.003</u>	20.352	35.718	0.009	20.819	33.415	37s	

Table 1. Comparison to SOTA methods in 2048 x 2048 and 4096 x 4096 resolution. The bold numbers denote the best performance and the underlined numbers denote the second best performance. ↑ and ↓ denote the higher the better and the lower the better respectively. We test the inference time on the same machine using a single NVIDIA A800 GPU.

[14], and AccDiffusion [31]. Except for SDXL+BSRGAN, which requires to use the trained BSRGAN model, other methods are training-free. We fix inference steps and set the negative prompts as empty. In addition, we remove additional tricks such as FreeU [48] for a fair comparison. Quantitatively, we mainly generate high-resolution images at target resolutions of 2048 x 2048 (4x of the original resolution) and 4096 x 4096 (16x of the original resolution).

We employ four widely used quantitative evaluation metrics: FID (Fréchet Inception Distance) [16], KID (Kernel Inception Distance) [3], IS (Inception Score) [45], and CLIP Score [41]. Specifically, FID_r, KID_r, and IS_r require resizing images to 299x299 before calculation. However, this kind of evaluation is not reasonable for high-resolution image generation. Following the approach of previous works [10, 31], we randomly crop 10 patches of 1024x1024 (1x) from each generated high-resolution image to further calculate FID_s, KID_c, and IS_c. For the 2048 x 2048 resolution scene, we set T_{min} at 40, T_{max} at 50, N at 1, ω_{min} at 30, ω_{max} at 30, M in Eq. 7 at 2 and M in Eq. 9 at 1. For the 4096 x 4096 resolution scene, we set T_{min} at 40, T_{max} at 50, N at 2, ω_{min} at 36.8, ω_{max} at 50, M in Eq. 7 at 0.5 and M in Eq. 9 at 0.5. Unless otherwise specified, all

of our evaluation experiments are conducted on NVIDIA-A800 GPUs.

4.2. Quantitative Results

As demonstrated in Tab. 1, our method achieves the best performance in 4 out of 8 metrics and the second best on 3 out of 8 metrics in 2048 x 2048 resolution scene, and achieves the best performance in 3 out of 8 metrics and the second best on 3 out of 8 metrics in 4096 x 4096 resolution scene, showing the effectiveness of RectifiedHR in solving the high-resolution generation task. Considering that our method requires the least time to generate a sample among all the training-free baselines in both 2048 x 2048 resolution and 4096 x 4096 resolution, it still produces high-resolution images with highly competitive performance, demonstrating the efficiency of our method. Although the SDXL+BSRGAN method is faster than ours, in cropped metrics, which are specifically designed for high-resolution generation, our method demonstrates superior performance compared to SDXL+BSRGAN at an acceptable additional time cost. In addition, we add the qualitative results for comparison with SDXL+BSRGAN in Fig. 8.

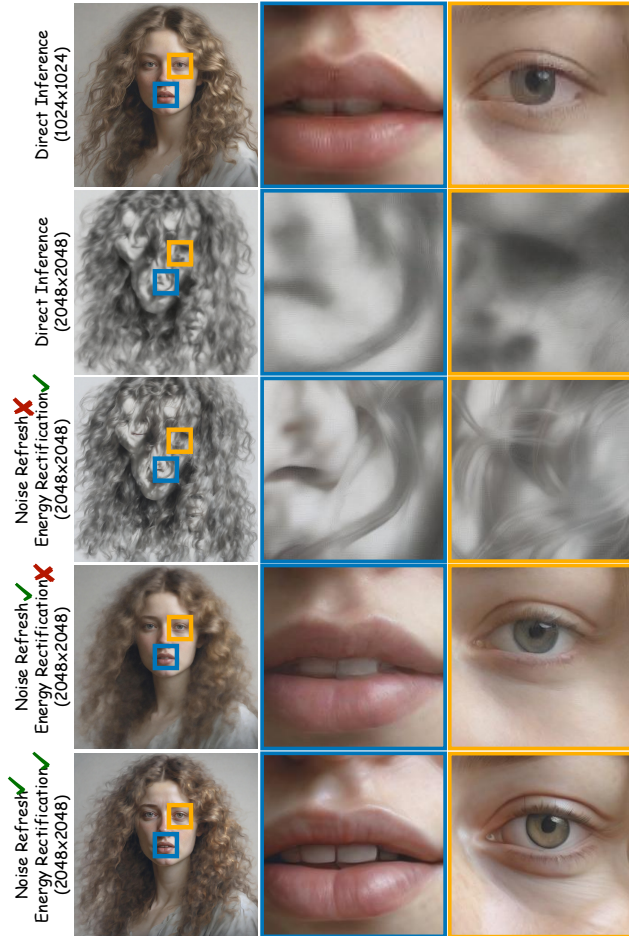


Figure 7. Ablation studies on our method.

4.3. Qualitative Results

To clearly observe the differences between our method and other baselines, we select three prompts from the LAION-5B dataset to conduct qualitative comparison experiments on FourwiScale, ScaleCrafter, DemoFusion, and HiDiffusion. In Fig. 6a, b, and c, we can observe that FouriScale exhibits abnormal high-frequency information, which masks the main subjects in the images, leading to a decrease in the quality of the generated images. In column b of Fig. 6, there is a noticeable edge blurring effect, which might be due to the window denoising mechanism of DemoFusion. From Fig. 6a, it can be seen that the car structures generated by ScaleCrafter are poor and also tend to produce blurred edges similar to Demofusion. It is evident that our method generates images with more reasonable edges and more accurate structures in Fig. 6.

4.4. Comparison with the super-resolution model.

To further compare the differences between the SDXL+BSRGAN and our method, we further com-



Figure 8. Qualitative Comparison between our method and SDXL+BSRGAN.

pare the qualitative results. The experimental setup is consistent with Sec. 4.1. As shown in Fig. 8, we find once the data generated by SDXL exceeds the domain of the original image, such as distorted faces, BSRGAN lacks the ability to correct these errors, leading to performance decline. Moreover, we consider our method and BSRGAN are not mutually exclusive. Some traditional super-resolution models, similar to BSRGAN, can help our training-free high-resolution image generation method add more details.

4.5. Ablation Study

Our method comprises two components: (i) noise refresh and (ii) energy rectification. To validate the effectiveness of these components, we perform experiments on all possible combinations, as illustrated in Fig. 7. The first and second rows in Fig. 7 represent images generated directly at resolutions of 1024 x 1024 and 2048 x 2048, respectively. It can be observed that when the 1024 x 1024 image is enlarged, there are local blurring phenomena. At the same time, it is evident that the 2048 x 2048 image in the second row of Fig. 7 exhibits repeated patterns and also suffers from blurring issues due to energy decay. The third row does not use noise refresh; instead, it only adds energy rectification in the last 15 steps of direct inference. Compared to the second row, although the repeated pattern problem is not resolved, the image becomes clearer. The fourth row introduces noise refresh but does not use energy rectification. It can be seen that noise refresh solves the repeated pattern problems found in the second and third rows, but there are still some blurring phenomena. The fifth row represents our method, which can be seen to solve both the repeated pattern problem and to make the details clearer.

5. Conclusion And Future Work

We propose an efficient and simple method called RectifiedHR for higher-resolution image generation. Specifically, we present a relative latent energy analysis and, to the best of our knowledge, are the first to identify the energy decay phenomenon during the high-resolution image generation process. We develop a novel training-free and easy pipeline for high-resolution image generation, which primarily consists of noise refresh and energy rectification

operations. Extensive comparisons show that RectifiedHR outperforms existing methods in terms of effectiveness and efficiency. However, our method has certain limitations; we have not yet adapted it to tasks beyond image generation. In the future, we plan to use our method in more tasks, such as image editing, video generation, and custom generation.

References

- [1] Omer Bar-Tal, Dolev Ofri-Amar, Rafail Fridman, Yoni Kasten, and Tali Dekel. Text2live: Text-driven layered image and video editing. In *ECCV*, pages 707–723. Springer, 2022. 1
- [2] Omer Bar-Tal, Lior Yariv, Yaron Lipman, and Tali Dekel. Multidiffusion: Fusing diffusion paths for controlled image generation. 2023. 1, 2, 3
- [3] Mikołaj Bińkowski, Danica J Sutherland, Michael Arbel, and Arthur Gretton. Demystifying mmd gans. *arXiv preprint arXiv:1801.01401*, 2018. 7
- [4] Tim Brooks, Aleksander Holynski, and Alexei A. Efros. Instructpix2pix: Learning to follow image editing instructions. In *CVPR*, pages 18392–18402, 2023. 1
- [5] Boyuan Cao, Jiaxin Ye, Yujie Wei, and Hongming Shan. Ap-ldm: Attentive and progressive latent diffusion model for training-free high-resolution image generation. *arXiv preprint arXiv:2410.06055*, 2024. 2, 4, 6
- [6] Junsong Chen, Jincheng Yu, Chongjian Ge, Lewei Yao, Enze Xie, Yue Wu, Zhongdao Wang, James Kwok, Ping Luo, Huchuan Lu, et al. Pixart-alpha: Fast training of diffusion transformer for photorealistic text-to-image synthesis. *arXiv preprint arXiv:2310.00426*, 2023. 1, 3
- [7] Junsong Chen, Chongjian Ge, Enze Xie, Yue Wu, Lewei Yao, Xiaoze Ren, Zhongdao Wang, Ping Luo, Huchuan Lu, and Zhenguo Li. Pixart-sigma: Weak-to-strong training of diffusion transformer for 4k text-to-image generation. In *European Conference on Computer Vision*, pages 74–91. Springer, 2025. 3
- [8] Guillaume Couairon, Jakob Verbeek, Holger Schwenk, and Matthieu Cord. Diffedit: Diffusion-based semantic image editing with mask guidance. 2022. 1
- [9] Ganggui Ding, Canyu Zhao, Wen Wang, Zhen Yang, Zide Liu, Hao Chen, and Chunhua Shen. Freecustom: Tuning-free customized image generation for multi-concept composition. In *Proceedings of the IEEE/CVF Conference on Computer Vision and Pattern Recognition*, pages 9089–9098, 2024. 1
- [10] Ruoyi Du, Dongliang Chang, Timothy Hospedales, Yi-Zhe Song, and Zhanyu Ma. Demofusion: Democratizing high-resolution image generation with no. In *Proceedings of the IEEE/CVF Conference on Computer Vision and Pattern Recognition*, pages 6159–6168, 2024. 2, 3, 6, 7
- [11] Patrick Esser, Sumith Kulal, Andreas Blattmann, Rahim Entezari, Jonas Müller, Harry Saini, Yam Levi, Dominik Lorenz, Axel Sauer, Frederic Boesel, et al. Scaling rectified flow transformers for high-resolution image synthesis. In *Forty-first International Conference on Machine Learning*, 2024. 1, 3
- [12] Rinon Gal, Yuval Alaluf, Yuval Atzmon, Or Patashnik, Amit H Bermano, Gal Chechik, and Daniel Cohen-Or. An image is worth one word: Personalizing text-to-image generation using textual inversion. *arXiv preprint arXiv:2208.01618*, 2022. 1
- [13] Moayed Haji-Ali, Guha Balakrishnan, and Vicente Ordonez. Elasticdiffusion: Training-free arbitrary size image generation through global-local content separation. In *Proceedings of the IEEE/CVF Conference on Computer Vision and Pattern Recognition*, pages 6603–6612, 2024. 2, 4, 6
- [14] Yingqing He, Shaoshu Yang, Haoxin Chen, Xiaodong Cun, Menghan Xia, Yong Zhang, Xintao Wang, Ran He, Qifeng Chen, and Ying Shan. Scalecrafter: Tuning-free higher-resolution visual generation with diffusion models. In *The Twelfth International Conference on Learning Representations*, 2023. 2, 3, 7
- [15] Jack Hessel, Ari Holtzman, Maxwell Forbes, Ronan Le Bras, and Yejin Choi. Clipscore: A reference-free evaluation metric for image captioning. 2021. 5
- [16] Martin Heusel, Hubert Ramsauer, Thomas Unterthiner, Bernhard Nessler, and Sepp Hochreiter. Gans trained by a two time-scale update rule converge to a local nash equilibrium. *Advances in neural information processing systems*, 30, 2017. 7
- [17] Jonathan Ho and Tim Salimans. Classifier-free diffusion guidance. *arXiv preprint arXiv:2207.12598*, 2022. 2, 4, 5
- [18] Jonathan Ho, Ajay Jain, and Pieter Abbeel. Denoising diffusion probabilistic models. *Advances in neural information processing systems*, 33:6840–6851, 2020. 3
- [19] Emiel Hoogeboom, Jonathan Heek, and Tim Salimans. simple diffusion: End-to-end diffusion for high resolution images. In *International Conference on Machine Learning*, pages 13213–13232. PMLR, 2023. 5
- [20] Linjiang Huang, Rongyao Fang, Aiping Zhang, Guanglu Song, Si Liu, Yu Liu, and Hongsheng Li. Fouriscale: A frequency perspective on training-free high-resolution image synthesis. In *European Conference on Computer Vision*, pages 196–212. Springer, 2025. 2, 3, 6
- [21] Juno Hwang, Yong-Hyun Park, and Junghyo Jo. Upsample guidance: Scale up diffusion models without training. *arXiv preprint arXiv:2404.01709*, 2024. 2, 4, 5
- [22] Zhiyu Jin, Xuli Shen, Bin Li, and Xiangyang Xue. Training-free diffusion model adaptation for variable-sized text-to-image synthesis. *Advances in Neural Information Processing Systems*, 36:70847–70860, 2023. 2, 3
- [23] Tero Karras, Miika Aittala, Timo Aila, and Samuli Laine. Elucidating the design space of diffusion-based generative models. *Advances in neural information processing systems*, 35:26565–26577, 2022. 3
- [24] Bahjat Kawar, Shiran Zada, Oran Lang, Omer Tov, Huiwen Chang, Tali Dekel, Inbar Mosseri, and Michal Irani. Imagic: Text-based real image editing with diffusion models. In *CVPR*, pages 6007–6017, 2023. 1
- [25] Younghyun Kim, Geunmin Hwang, Junyu Zhang, and Eunbyung Park. Diffusehigh: Training-free progressive high-resolution image synthesis through structure guidance. *arXiv preprint arXiv:2406.18459*, 2024. 2, 4, 6

- [26] Black Forest Labs. Flux. <https://github.com/black-forest-labs/flux>, 2023. 1, 3
- [27] Yuseung Lee, Kunho Kim, Hyunjin Kim, and Minhyuk Sung. Syncdiffusion: Coherent montage via synchronized joint diffusions. *Advances in Neural Information Processing Systems*, 36:50648–50660, 2023. 2, 3
- [28] Dongxu Li, Junnan Li, and Steven Hoi. Blip-diffusion: Pre-trained subject representation for controllable text-to-image generation and editing. *Advances in Neural Information Processing Systems*, 36, 2024. 1
- [29] Zhimin Li, Jianwei Zhang, Qin Lin, Jiangfeng Xiong, Yanxin Long, Xincheng Deng, Yingfang Zhang, Xingchao Liu, Minbin Huang, Zedong Xiao, et al. Hunyuan-dit: A powerful multi-resolution diffusion transformer with fine-grained chinese understanding. *arXiv preprint arXiv:2405.08748*, 2024. 1, 3
- [30] Mingbao Lin, Zhihang Lin, Wengyi Zhan, Liujuan Cao, and Rongrong Ji. Cutdiffusion: A simple, fast, cheap, and strong diffusion extrapolation method. *arXiv preprint arXiv:2404.15141*, 2024. 2, 3, 6
- [31] Zhihang Lin, Mingbao Lin, Meng Zhao, and Rongrong Ji. Accdiffusion: An accurate method for higher-resolution image generation. In *European Conference on Computer Vision*, pages 38–53. Springer, 2025. 2, 3, 7
- [32] Yaron Lipman, Ricky TQ Chen, Heli Ben-Hamu, Maximilian Nickel, and Matt Le. Flow matching for generative modeling. *arXiv preprint arXiv:2210.02747*, 2022. 3
- [33] Mushui Liu, Yuhang Ma, Yang Zhen, Jun Dan, Yunlong Yu, Zeng Zhao, Zhipeng Hu, Bai Liu, and Changjie Fan. Llm4gen: Leveraging semantic representation of llms for text-to-image generation. *arXiv preprint arXiv:2407.00737*, 2024. 1
- [34] Xingchao Liu, Chengyue Gong, and Qiang Liu. Flow straight and fast: Learning to generate and transfer data with rectified flow. *arXiv preprint arXiv:2209.03003*, 2022. 3
- [35] Xinyu Liu, Yingqing He, Lanqing Guo, Xiang Li, Bu Jin, Peng Li, Yan Li, Chi-Min Chan, Qifeng Chen, Wei Xue, et al. Hiprompt: Tuning-free higher-resolution generation with hierarchical mllm prompts. *arXiv preprint arXiv:2409.02919*, 2024. 2, 4
- [36] Simian Luo, Yiqin Tan, Longbo Huang, Jian Li, and Hang Zhao. Latent consistency models: Synthesizing high-resolution images with few-step inference. *arXiv preprint arXiv:2310.04378*, 2023. 1, 3
- [37] Chenlin Meng, Yutong He, Yang Song, Jiaming Song, Jiajun Wu, Jun-Yan Zhu, and Stefano Ermon. Sdedit: Guided image synthesis and editing with stochastic differential equations. *arXiv preprint arXiv:2108.01073*, 2021. 2, 4
- [38] Daiki Miyake, Akihiro Iohara, Yu Saito, and Toshiyuki Tanaka. Negative-prompt inversion: Fast image inversion for editing with text-guided diffusion models. 2023. 1
- [39] Ron Mokady, Amir Hertz, Kfir Aberman, Yael Pritch, and Daniel Cohen-Or. Null-text inversion for editing real images using guided diffusion models. In *CVPR*, pages 6038–6047, 2023. 1
- [40] Dustin Podell, Zion English, Kyle Lacey, Andreas Blattmann, Tim Dockhorn, Jonas Müller, Joe Penna, and Robin Rombach. Sdxl: Improving latent diffusion models for high-resolution image synthesis. *arXiv preprint arXiv:2307.01952*, 2023. 1, 3, 4, 6
- [41] Alec Radford, Jong Wook Kim, Chris Hallacy, Aditya Ramesh, Gabriel Goh, Sandhini Agarwal, Girish Sastry, Amanda Askell, Pamela Mishkin, Jack Clark, et al. Learning transferable visual models from natural language supervision. In *International conference on machine learning*, pages 8748–8763. PMLR, 2021. 7
- [42] Robin Rombach, Andreas Blattmann, Dominik Lorenz, Patrick Esser, and Björn Ommer. High-resolution image synthesis with latent diffusion models. In *Proceedings of the IEEE/CVF conference on computer vision and pattern recognition*, pages 10684–10695, 2022. 1, 3
- [43] Olaf Ronneberger, Philipp Fischer, and Thomas Brox. U-net: Convolutional networks for biomedical image segmentation. In *Medical image computing and computer-assisted intervention—MICCAI 2015: 18th international conference, Munich, Germany, October 5–9, 2015, proceedings, part III 18*, pages 234–241. Springer, 2015. 3
- [44] Nataniel Ruiz, Yuanzhen Li, Varun Jampani, Wei Wei, Tingbo Hou, Yael Pritch, Neal Wadhwa, Michael Rubinstein, and Kfir Aberman. Hyperdreambooth: Hypernetworks for fast personalization of text-to-image models. *arXiv preprint arXiv:2307.06949*, 2023. 1
- [45] Tim Salimans, Ian Goodfellow, Wojciech Zaremba, Vicki Cheung, Alec Radford, and Xi Chen. Improved techniques for training gans. *Advances in neural information processing systems*, 29, 2016. 7
- [46] Christoph Schuhmann, Romain Beaumont, Richard Vencu, Cade Gordon, Ross Wightman, Mehdi Cherti, Theo Coombes, Aarush Katta, Clayton Mullis, Mitchell Wortsman, et al. Laion-5b: An open large-scale dataset for training next generation image-text models. *Advances in Neural Information Processing Systems*, 35:25278–25294, 2022. 5, 6
- [47] Shuwei Shi, Wenbo Li, Yuechen Zhang, Jingwen He, Biao Gong, and Yinqiang Zheng. Resmaster: Mastering high-resolution image generation via structural and fine-grained guidance. *arXiv preprint arXiv:2406.16476*, 2024. 2, 4
- [48] Chenyang Si, Ziqi Huang, Yuming Jiang, and Ziwei Liu. Freeu: Free lunch in diffusion u-net. In *Proceedings of the IEEE/CVF Conference on Computer Vision and Pattern Recognition*, pages 4733–4743, 2024. 7
- [49] Jiaming Song, Chenlin Meng, and Stefano Ermon. Denoising diffusion implicit models. *arXiv preprint arXiv:2010.02502*, 2020. 3, 5
- [50] Yang Song, Jascha Sohl-Dickstein, Diederik P Kingma, Abhishek Kumar, Stefano Ermon, and Ben Poole. Score-based generative modeling through stochastic differential equations. *arXiv preprint arXiv:2011.13456*, 2020. 3
- [51] Yoad Tewel, Rinon Gal, Gal Chechik, and Yuval Atzmon. Key-locked rank one editing for text-to-image personalization. In *ACM SIGGRAPH 2023 Conference Proceedings*, 2023. 1
- [52] Narek Tumanyan, Michal Geyer, Shai Bagon, and Tali Dekel. Plug-and-play diffusion features for text-driven

- image-to-image translation. In *CVPR*, pages 1921–1930, 2023. 1
- [53] Haoning Wu, Shaocheng Shen, Qiang Hu, Xiaoyun Zhang, Ya Zhang, and Yanfeng Wang. Megafusion: Extend diffusion models towards higher-resolution image generation without further tuning. *arXiv preprint arXiv:2408.11001*, 2024. 2, 4
- [54] Zhen Yang, Ganggui Ding, Wen Wang, Hao Chen, Bohan Zhuang, and Chunhua Shen. Object-aware inversion and reassembly for image editing. *arXiv preprint arXiv:2310.12149*, 2023. 1
- [55] Kai Zhang, Jingyun Liang, Luc Van Gool, and Radu Timofte. Designing a practical degradation model for deep blind image super-resolution. In *Proceedings of the IEEE/CVF International Conference on Computer Vision*, pages 4791–4800, 2021. 6
- [56] Shen Zhang, Zhaowei Chen, Zhenyu Zhao, Zhenyuan Chen, Yao Tang, Yuhao Chen, Wengang Cao, and Jiajun Liang. Hidiffusion: Unlocking high-resolution creativity and efficiency in low-resolution trained diffusion models. *arXiv preprint arXiv:2311.17528*, 2023. 2, 3, 6
- [57] Zhengqiang Zhang, Ruihuang Li, and Lei Zhang. Frecas: Efficient higher-resolution image generation via frequency-aware cascaded sampling. *arXiv preprint arXiv:2410.18410*, 2024. 2, 4, 6
- [58] Le Zhuo, Ruoyi Du, Han Xiao, Yangguang Li, Dongyang Liu, Rongjie Huang, Wenzhe Liu, Lirui Zhao, Fu-Yun Wang, Zhanyu Ma, et al. Lumina-next: Making lumina-t2x stronger and faster with next-dit. *arXiv preprint arXiv:2406.18583*, 2024. 1, 3